JOURNAL OF THE AMERICAN CHEMICAL SOCIETY

Subscriber access provided by Karolinska Institutet, University Library

Article

Twofold #-Extension of Polyarenes via Double and Triple Radical Alkyne peri-Annulations: Radical Cascades Converging on the Same Aromatic Core

Edgar Gonzalez-Rodriguez, Miguel A. Abdo, Gabriel dos Passos Gomes, Suliman Ayad, Frankie D. White, Nikolay P. Tsvetkov, Kenneth Hanson, and Igor Alabugin

J. Am. Chem. Soc., **Just Accepted Manuscript** • DOI: 10.1021/jacs.0c01856 • Publication Date (Web): 04 Apr 2020

Downloaded from pubs.acs.org on April 5, 2020

Just Accepted

“Just Accepted” manuscripts have been peer-reviewed and accepted for publication. They are posted online prior to technical editing, formatting for publication and author proofing. The American Chemical Society provides “Just Accepted” as a service to the research community to expedite the dissemination of scientific material as soon as possible after acceptance. “Just Accepted” manuscripts appear in full in PDF format accompanied by an HTML abstract. “Just Accepted” manuscripts have been fully peer reviewed, but should not be considered the official version of record. They are citable by the Digital Object Identifier (DOI®). “Just Accepted” is an optional service offered to authors. Therefore, the “Just Accepted” Web site may not include all articles that will be published in the journal. After a manuscript is technically edited and formatted, it will be removed from the “Just Accepted” Web site and published as an ASAP article. Note that technical editing may introduce minor changes to the manuscript text and/or graphics which could affect content, and all legal disclaimers and ethical guidelines that apply to the journal pertain. ACS cannot be held responsible for errors or consequences arising from the use of information contained in these “Just Accepted” manuscripts.

is published by the American Chemical Society. 1155 Sixteenth Street N.W., Washington, DC 20036

Published by American Chemical Society. Copyright © American Chemical Society. However, no copyright claim is made to original U.S. Government works, or works produced by employees of any Commonwealth realm Crown government in the course of their duties.

Twofold π-Extension of Polyarenes via Double and Triple Radical Alkyne *peri*-Annulations: Radical Cascades Converging on the Same Aromatic Core

Edgar Gonzalez-Rodriguez, Miguel A. Abdo, Gabriel dos Passos Gomes[§], Suliman Ayad, Frankie D. White[§§], Nikolay P. Tsvetkov, Kenneth Hanson and Igor V. Alabugin*

Department of Chemistry and Biochemistry, Florida State University, Tallahassee, Florida 32306-4390, United States.

S *Supporting Information*

ABSTRACT: A versatile synthetic route to distannyl-substituted polyarenes was developed via double radical *peri*-annulations. The cyclization precursors were equipped with propargylic OMe traceless directing groups (TDGs) for regioselective Sn-radical attack at the triple bonds. The two *peri*-annulations converge at a variety of polycyclic cores to yield expanded difunctionalized polycyclic aromatic hydrocarbons (PAHs). This approach can be extended to *triple peri*-annulations, where annulations are coupled with a radical cascade that connects *two* preexisting aromatic cores via a formal C-H activation step.

The installed Bu_3Sn groups serve as chemical handles for further functionalization via direct cross-coupling, iodination, or protodestannylation, and increase solubility of the products in organic solvents. Photophysical studies reveal that the Bu_3Sn-substituted PAHs are moderately fluorescent, and their protodestannylation results in an up to 10-fold fluorescence quantum yield enhancement. DFT calculations identified the most likely possible mechanism of this complex chemical transformation involving two independent *peri*-cyclizations at the central core.

INTRODUCTION

Nanographenes (NGs), large polycyclic aromatic hydrocarbons (PAHs), and graphene nanoribbons (GNRs) have found widespread applications in optoelectronic devices.[1–10] The broad interest in these carbon-rich molecules stems from their promising physical properties, which can be modulated through their size, edge topology, and substitution.[11–14]

Synthetic top-down approaches to GNRs generally lack the precision needed to achieve uniform widths and well-defined edge structures. On the other hand, bottom-up protocols which build NGs and GNRs from small PAH building blocks build size and complexity in a controlled fashion.[15–31] The synthetic toolset available for the bottom-up preparation and modification of PAHs, NGs, and GNRs expands continuously to fine-tune their electronic properties and improve their solubility and processability. The high energy content and carbon-richness of alkynes makes them a privileged functional group within this reaction toolset.[32–45] Yet, most of the available examples of alkynes being used in the preparation of these carbon-rich molecules concentrate on extension at the armchair edge of the polycyclic framework, while alkyne annulations at the zigzag edge remain remarkably scarce (Scheme 1).[46,47]

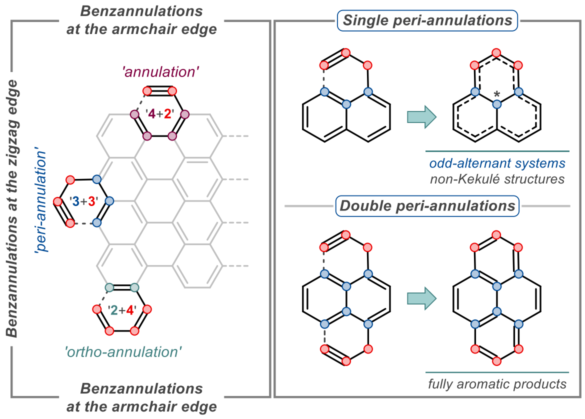

Scheme 1. Left: *peri*-annulations allow benzannulations at the zigzag edge of polyarenes. Right: single *peri*-annulations produce odd-alternant polycyclic systems that are not classic Kekulé structures. Double *peri*-annulations give rise to ‘normal’ aromatic products. * = radical, cation, anion.

Recently, our group reported radical *peri*-annulations at the zigzag edge of acene moieties through a traceless directing group (TDG) approach.[48] In the past, this strategy allowed for the synthesis of fused helicenes and ‘defect-free’ polycyclic aromatics in a modular and scalable way.[49–52] In these transformations, the TDG serves two critical roles. First, it ensures the chemo- and regioselective Sn-attack at the desired alkyne carbon. Second, it facilitates the final aromatization step of the reaction cascade by undergoing β-radical elimination (Scheme 2a). The TDG-guided *peri*-cyclizations allow for the zigzag edge extension of various acene precursors via benzannulation. The initially formed cyclic products can be trapped by either oxidative or non-oxidative pathways giving rise to polycyclic ketones or destannylated derivatives, respectively (Scheme 2b).

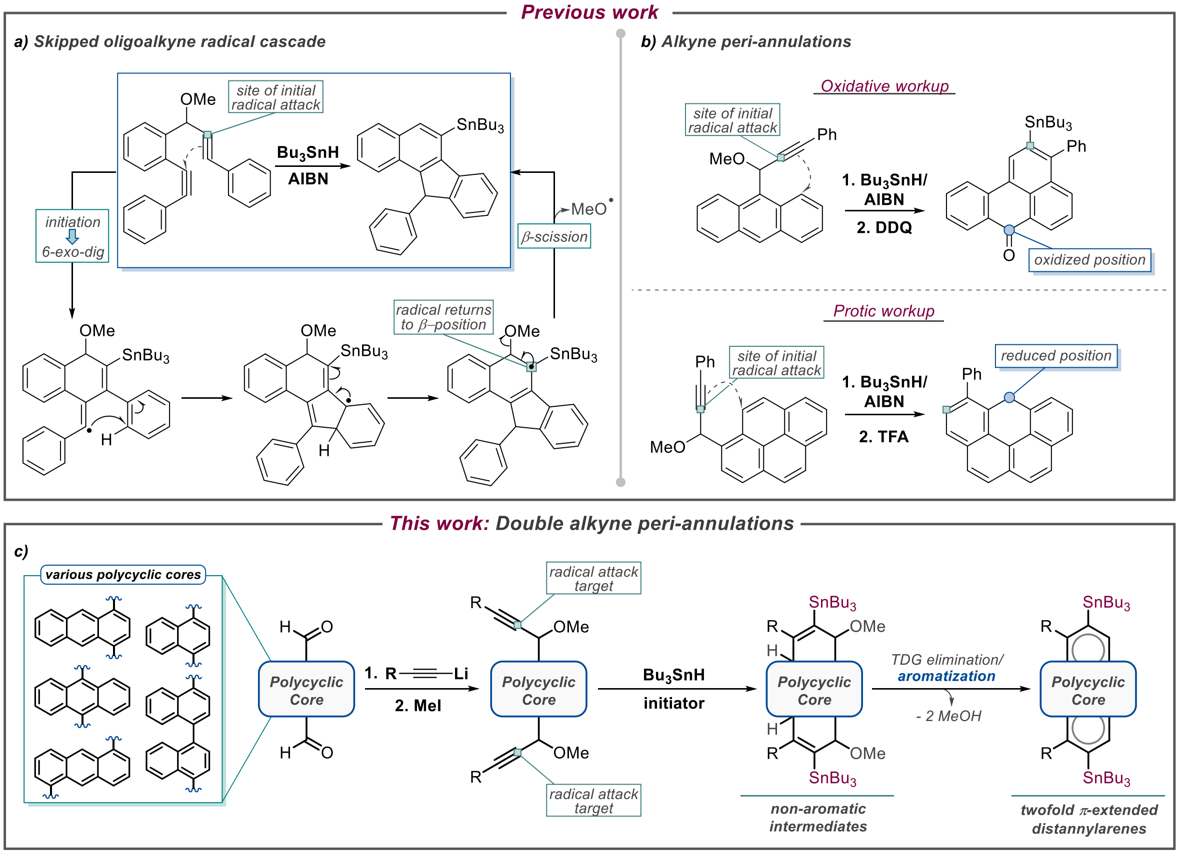

Scheme 2. Evolution of the MeO-TDG guided Sn-radical cyclizations. a) TDG in radical cascades: from skipped oligoalkynes to fused helicenes. b) Radical alkyne *peri*-annulation reactions at the L-region of acenes. c) Double alkyne *peri*-annulations for the preparation of diverse PAHs.

Herein, we disclose how two TDG-guided *peri*-annulations can start at opposite termini and *converge* at a common polycyclic core. Not only does the dual cascade of radical *peri*-annulations achieve the twofold π-extension at zigzag edges of PAHs (Scheme 2c), but it also—in contrast to our previous work—circumvents the need for external oxidizing or reducing agents. Unlike the single *peri*-cyclization that provides a non-Kekulé polycyclic system with an odd number of carbons, the products of the double *peri*-cascade can undergo full aromatization simply through the elimination of MeOH (derived from the TDG). In this design, the TDG takes an additional role: not only does its presence assist in the selective cascade initiation but its departure also terminates the reaction, aromatizing the ring. Furthermore, the newly installed Bu_3Sn groups increase solubility and open up avenues for further downstream derivatization.

RESULTS AND DISCUSSION

Our exploration of the double *peri*-annulation started with the naphthalene system. The model bis-propargyl derivative **1b** was prepared from naphthalene-1,4-dicarbaldehyde in a one-pot procedure that included the nucleophilic addition of lithium acetylide to the aldehyde followed by quenching with MeI (Scheme 3). Subjecting **1b** to the initial cyclization conditions gave rise to the desired 1,8-diphenyl-2,7-distannylpyrene (**2b**) in a 7% yield with 11% unreacted starting material recovered (Table 1, entry 1). Attempts to isolate and identify side products were unfruitful given the low quantities in which they are formed as well as their instability. Inspection of the NMR spectrum of the reaction mixture suggests that the competing reactions are numerous and non-specific. Nevertheless, despite the low yield, the target distannylpyrene was formed as the major isolable product.

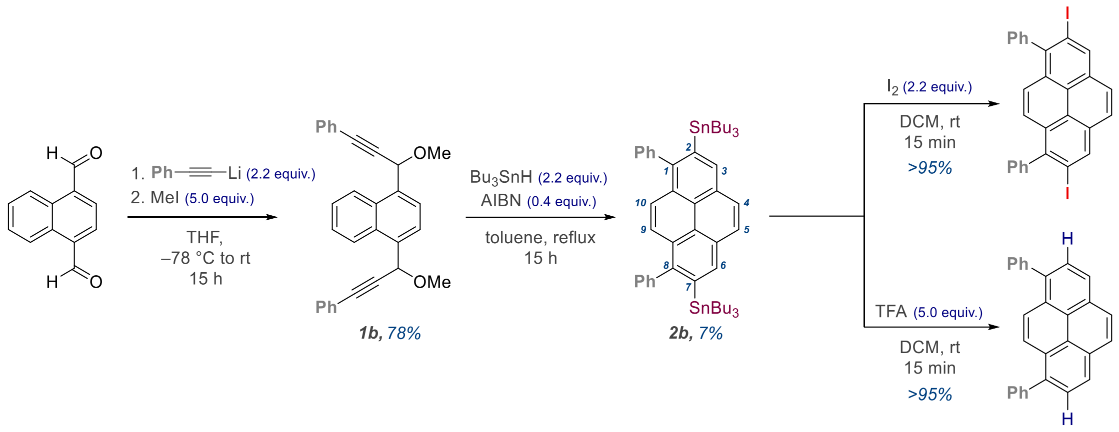

Scheme 3. Double *peri*-annulation on the naphthalene system and numbering for the pyrene core.

With this initial result, we searched for the optimal reaction conditions with alkyne **1b** as the substrate (Table 1 and S1). First, we found that an increase in the amount of initiator helped to achieve full starting material conversion and increase pyrene formation (Table 1, entry 2). Replacing 2,2′-azobis(2-methylpropionitrile) (AIBN) for non-azo thermal initiators led to sluggish and non-specific decomposition of the starting material (Table S1). In contrast, yields improved when the more thermally stable 1,1′-azobis(cyclohexanecarbonitrile) (ACHN) initiator was used (Table 1, entries 3-5). The correlation between equivalents of initiator and the increase in desired product formation tapered off at initiator loads exceeding 1.6 equivalents. These observations suggest that the radical chain propagation in this reaction is inefficient. Furthermore, the thermal initiator may play a second role where it functions as an oxidizing agent in a hydrogen-atom abstraction event at a later reaction stage.[53]

To explore whether oligomerization could impact the yields, we varied the initial concentration of the starting material. Slight dilution (0.02 M reactant concentration) was better than the initial conditions (entry 6). However, further dilution proved to be counterproductive (0.01 M, entry 7). NMR analysis showed that the formation of product is stopped after 5 hours, even when side reactions seem to be progressing—evidenced by color changes and TLC variations. A switch from toluene to aromatic solvents that lack labile C-H bonds was used to probe for the possible involvement of H-atom abstraction as a side reaction decreasing the product yield (entries 9, 10, and SI). However, the use of α,α,α-trifluorotoluene (entry 9) slightly lowered the yield of the desired product. Also, the use of *o*-dichlorobenzene along with higher reaction temperatures (140 ˚C) was detrimental for the desired reaction (entry 10).

The importance of the directing interaction between the OMe group and Sn-centered radicals, a process that briefly became controversial before being convincingly addressed by Hale and coworkers,[54–60] was confirmed by testing various radical sources. Sn-centered radicals (Ph_3SnH or Bu_3SnH) substantially outperformed other radical sources (Si-centered radicals, Togni II, and $RB(OH)_2/Mn^{III}$). The use of different propargyl ether TDGs also lowered the reaction yields (Table S1).

Finally, we probed the stability of the product by subjecting compound **2b** to the optimized reaction conditions. No decomposition occurred after 15 hours, and the starting material was recovered in its entirety (Table S1).

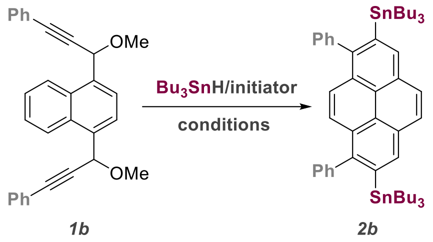

Entry	Reagent (equiv.)	Initiator (equiv.)	Conditions	Yield
1[a]	Bu_3SnH (2.2)	AIBN (0.4)	toluene, reflux, 15 h	7%*
2[a]	Bu_3SnH (2.2)	AIBN (0.8)	toluene, reflux, 15 h	21%
3[a]	Bu_3SnH (2.2)	ACHN (0.8)	toluene, reflux, 15 h	22%
4[a]	Bu_3SnH (2.2)	ACHN (1.2)	toluene, reflux, 15 h	26%
5[a]	Bu_3SnH (2.2)	ACHN (1.6)	toluene, reflux, 15 h	31%
6[b]	**Bu_3SnH (2.2)**	**ACHN (1.6)**	**toluene, reflux, 5 h**	**38%**
7[c]	Bu_3SnH (2.2)	ACHN (1.6)	toluene, reflux, 15 h	18%
8[b]	Bu_3SnH (4.0)	ACHN (1.6)	toluene, reflux, 15 h	37%
9[b]	Bu_3SnH (2.2)	ACHN (1.6)	$PhCF_3$, reflux,15 h	29%
10[b]	Bu_3SnH (2.2)	ACHN (1.6)	ODCB, 140 ˚C,15 h	10%

Table 1. Optimization of the Sn-promoted double radical cyclization of alkyne **1b**. Initial Starting material concentration: [a] 0.04 M, [b] 0.02 M, and [c] 0.01 M. *conversion for entry 1 was 89%. ODCB= *o*-Dichlorobenzene. Bu_3SnH/initiator mixtures were added over the course of 3 hours via syringe pump.

With the optimized conditions in hand, we evaluated the reaction scope by preparing a selection of 1,4-disubstituted naphthalenes and subjecting them to the reaction conditions. Through our method, a series of 1,8-disubstituted-2,7-distannylpyrenes were prepared in moderate yields (Scheme 4, products **2a-e**). The reaction was tolerant for alkyl substituents, extended aromatics, and electron-donating groups (**2a**, **2c**, and **2d**, respectively). The presence of a nitrile substituent negatively impacted the reaction yield (24% of **2e**), possibly due to the undesired reactivity of nitriles towards radicals as a competing reaction.

To our knowledge, this is the first report where the 1,2,7,8-substitution pattern on pyrenes is accessed straightforwardly (Scheme 3). In order to obtain the closest analog (i.e., 1,8-disubstituted pyrenes), multiple separations from its 1,6-isomer are required.[61] Additionally, with our approach, the two Sn-functionalities in the cyclized products serve as solubilizing groups and chemical handles for further derivatization. For example, reacting the distannypyrenes with I_2 transforms them into their diiodo counterparts (**3a-e**). This polarity reversal—from nucleophilic to electrophilic—expands the possibilities for their derivatization through cross-coupling transformations (e.g., Stille, Suzuki, and Sonogashira). Similarly, protodestannylation of the distannylpyrenes gives access, in near-quantitative yields, to compounds **4a-e** where the Bu_3Sn groups have been removed. This ability to remove Sn groups with acid may be used as a precipitation technique for depositing these conjugated molecules out of solution with good degree of spatial control.

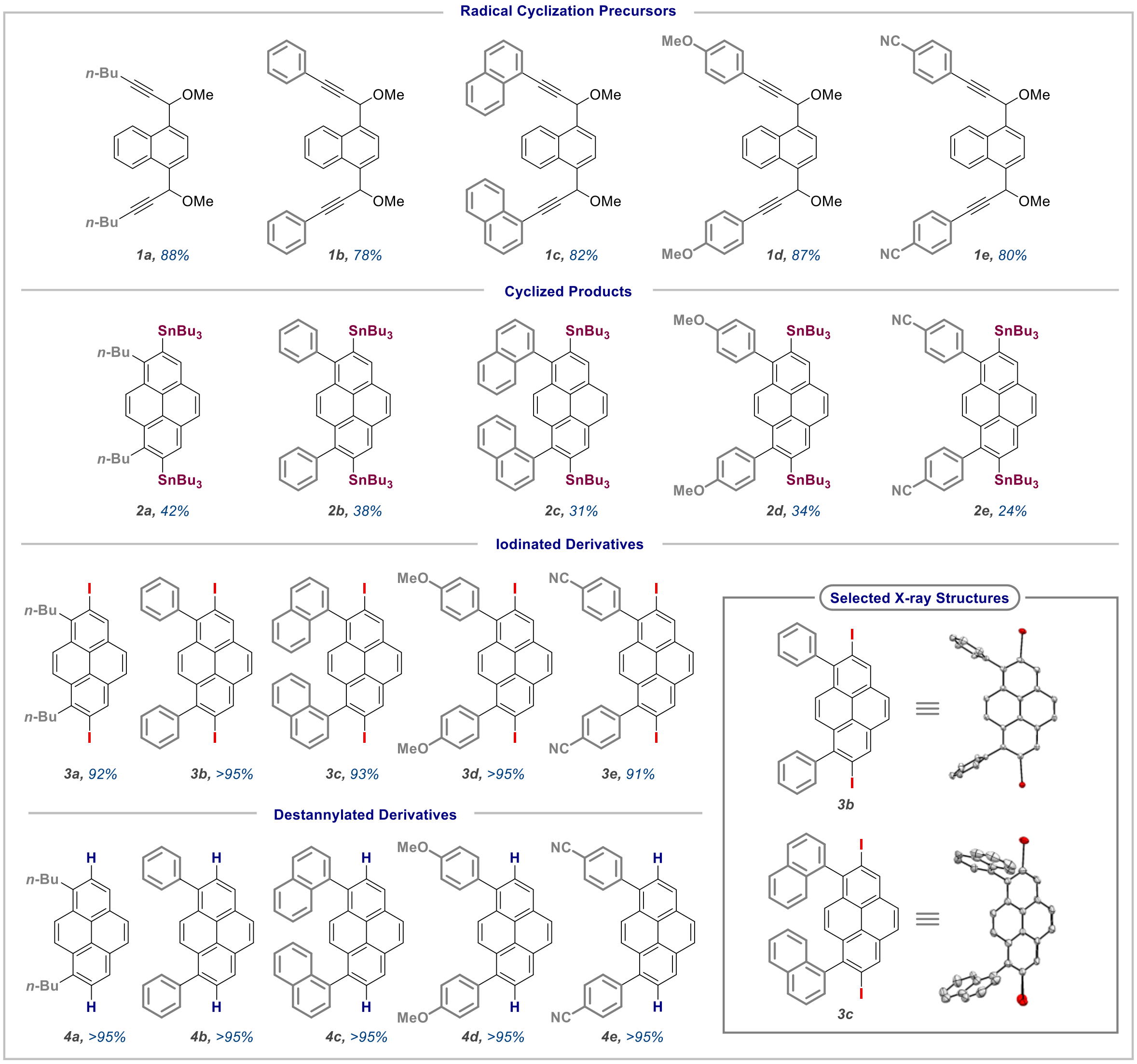

Scheme 4. Synthesis of 1,8-substituted-2,7-bis-stannylpyrenes through the Sn-radical cyclization approach and their derivatization to the iodinated and destannylated products.

In the next step, we explored the expansion of the double *peri*-annulation to larger polycyclic cores. With anthracene, an added layer of diversification for accessible products is introduced. Depending on where the pendant propargyl-ether groups are located on the starting material (i.e. 1,4—1,5 or 9,10), the products of the bis-cyclization can give 2,7-bis(tributylstannyl)benzo[*e*]pyrenes or 2,8-bis(tributylstannyl)perylenes (Scheme 5, products **2g** and **2h**, respectively).

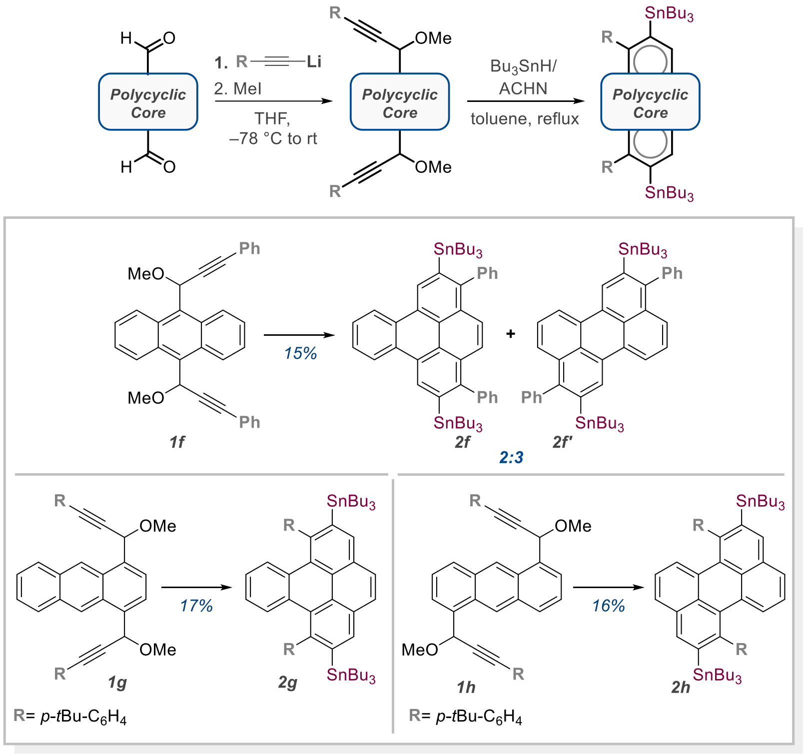

Scheme 5. Expansion of the *peri*-annulations to different polycyclic aromatic cores. Unoptimized yields reported.

For the 9,10-anthracene propargyl ether **1f,** two isomeric polycyclic products were formed (benzo[e]pyrene **2f** and perylene **2f'**) in a 2 to 3 ratio. Although the two products coelute from column chromatography, crystals of **2f'** can be grown from the two-component mixture. Single crystal X-ray analysis confirmed the perylene structure of **2f'**. The solid-state structure of this compound shows that the presence of bulky Bu_3Sn groups forces the perylene moiety to pack in staggered sheets to allow for the perpendicular contortion of the neighboring phenyl groups (~96° dihedral in Scheme 6). With this geometric feature, conjugation from the phenyl groups into the central core is broken, and potential π–π interactions between the perylene groups are thwarted.

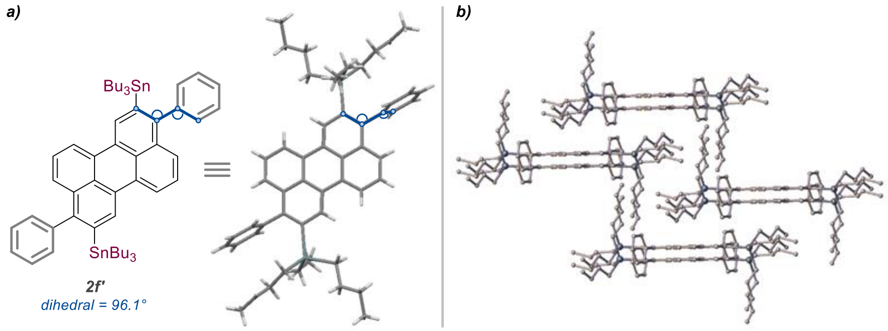

Scheme 6. a) X-ray structure for compound **2f'**. b) Crystal packing of compound **2f'**.

Triple *peri*-cyclization: combination of non-oxidative and oxidative aromatization strategies

In addition to the expansion of the double *peri*-annulations to anthracene, we explored the preparation of peropyrenes through a ***triple*** *peri*-cyclization of bis-naphthalene **1i** (Scheme 7). For the earlier extended cyclizations where two vinyl radicals converge on a single core, full aromatization is readily achieved via the loss of two MeOH molecules. Hence, no additional reduction or oxidation is needed. In contrast, for substrate **1i**, the partially aromatized polycycle generated after elimination of the TDGs must undergo dehydrogenative oxidation to form the final product (Scheme 7). We were encouraged by precedent from our lab where a similar oxidation step was accomplished by using an excess of the radical initiator.[53] Gratifyingly, the triple *peri*-annulation on the bis-naphthyl precursor **1i** successfully proceeded all the way to bis(tributylstannyl)peropyrene **2i** under this operationally simple one-pot procedure. The 11% yield of the final product corresponds to a ~75% yield per elementary step. Further optimization of the reaction conditions for this system will be pursued in the future.

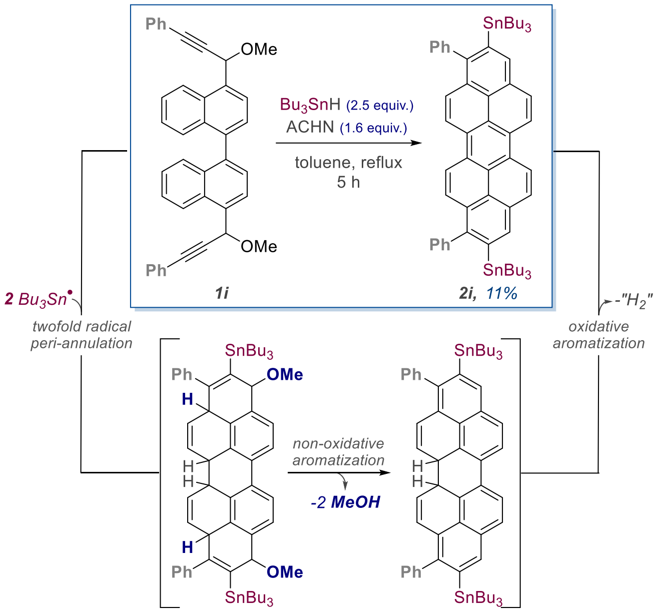

Scheme 7. *Triple* radical *peri*-annulation for binaphthalene **1i** where an extra *in situ* oxidation step converts a binaphthyl moiety into a perylene core on route to the peropyrene product **2i**.

The triple *peri*-annulation couples the two Sn-radical initiated non-oxidative cyclizations with an additional oxidative cyclization. The *in situ* oxidation step with ACHN-derived radicals, that converts the binaphthyl moiety into a perylene core en route to the final peropyrene product, is synthetically equivalent to the Scholl reaction but without the need for a harsh oxidant (e.g., $FeCl_3$).

Strategies for further synthetic expansions

Like their pyrene counterparts, the distannylperopyrenes, benzopyrenes, and perylenes can be easily converted to the diiodo and destannylated analogues in excellent yields (see SI). Furthermore, the diiodo polyarenes offer multiple opportunities for the rapid π-extension of polycyclic frameworks (Scheme 8). Here, the modularity of the R groups and cross-coupling partners allows for the design of reaction sequences that give access to extended polysubstituted polyarenes.

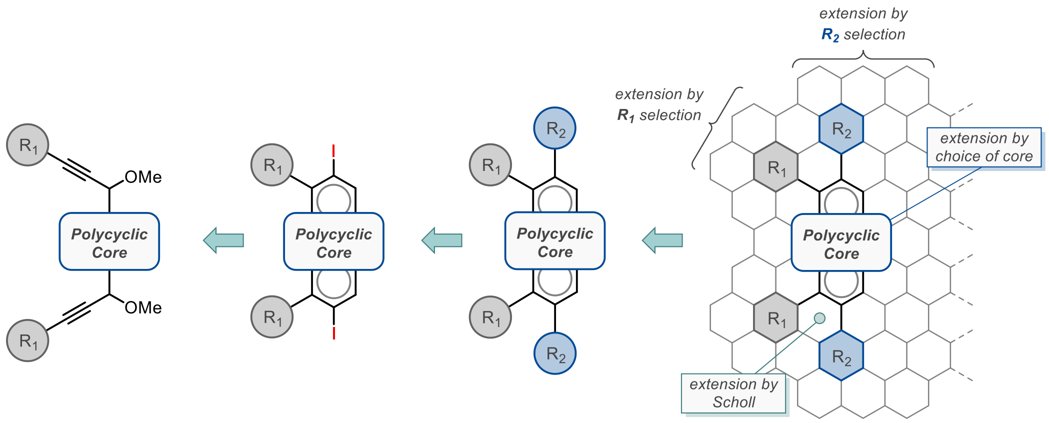

Scheme 8. Double *peri*-annulation approach for the rapid construction of extended PAHs.

As a proof-of-concept for such opportunities, we have used a *peri*-annulation/cross-coupling/cyclodehydrogenation cascade to prepare the decacyclic product **10**, which can be considered a fusion of two phenanthrene moieties on a pyrene core (Scheme 9). In this instance, the original phenyl group was switched for a 4-*tert*-butylphenyl group that can improve solubility for the later steps of the synthetic sequence. The substituent selection on the 1, 2, 7, and 8 positions also allow for a final cycloaromatization reaction to access fully conjugated products. This way, diiodinated product **3j** was prepared from compound **1j** (1.89 mmol) on a gram scale through a one-pot *peri*-annulation/iodination sequence (32% yield). An advantage of the diiodo derivatives over their distannyl counterparts is their increased stability during column chromatography. A double Suzuki cross-coupling of the diiodide **3j** with 4-*tert*-butylphenylboronic acid proceeded in excellent yield (80%) to produce tetrakis(4-(*tert*-butyl)phenyl)pyrene **9**. In the final step, the latter was cyclized to the target compound **10** through a Scholl reaction in a 59% yield (4 steps from **1j**; 15% overall yield).[62] One can envision how the choice of the central aromatic core, R groups, and cross-coupling partners would allow for the access of a vast number of carbon-rich structures. Similarly, oligomerization and polymerization through cross-coupling of the electrophilic and nucleophilic building blocks can, in principle, provide a modular approach to novel NG and GNR architectures. Several topologies could be readily accessible by mixing and matching the difunctionalized polyarene building blocks available through this method. Efforts are underway by our group in these directions.

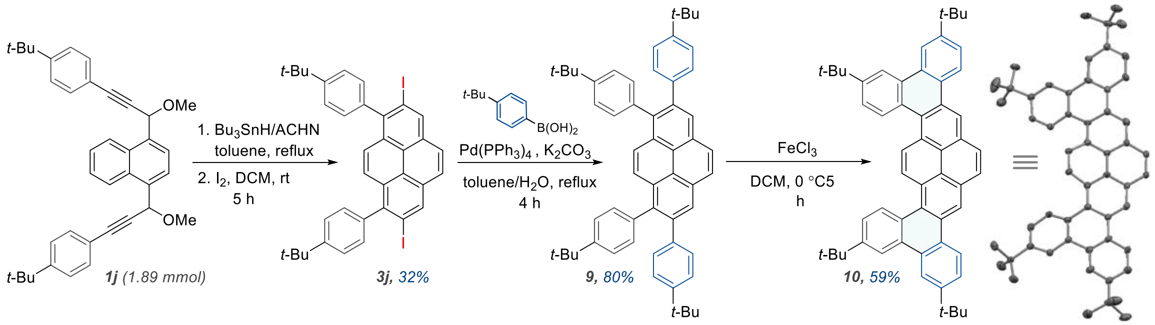

Scheme 9. Preparation of 2,11,14,21-tetra-*tert*-butylpentabenzo[*a*,*c*,*m*,*o*,*rst*]pentaphene **10** starting from cyclization precursor **1j**; X-ray structure of compound **10**.

Photophysical Properties

Pyrenes and peropyrenes are among the most popular chromophores. They often have high fluorescence quantum yields, form long-lived singlet excited states, and display interesting photophysical features such as excimer and exciplex formation.[63,64] These properties have led to a broad range of applications, including organic light-emitting diodes (OLEDs), organic field-effect transistors (OFETs), and organic photovoltaic cells (OPVs).[65] Furthermore, pyrenes have been used as sensors for temperature, pressure, pH, and a variety of chemical analytes.[66] Peropyrenes are also of high interest as potential singlet fission chromophores.[67,68]

The new synthetic route reported here allows, for the first time, access a previously unavailable substitution pattern that breaks the symmetry of the pyrene core and introduces polarization to its π-system.

Table **2** contains a summary of the photophysical properties of a representative group of the new polycyclic products.

Our investigation began with the pyrene series shown in Scheme 4. In general, the pyrene series presents absorption and emission features that are mirror images of each other, indicating that the same electronic states are involved in both phenomena (i.e., absorption and emission; Figure 1, left) with Stoke's shifts that range from 1940-3950 cm^{-1}.

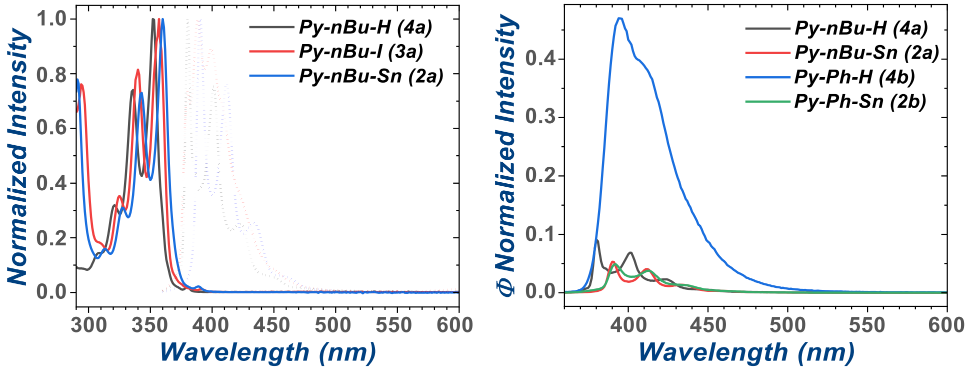

Figure 1. Left: Normalized absorption (solid line) and emission (dashed line) spectra for the *n*Bu-substituted pyrene family. Right: Emission spectra for *n*Bu-pyrenes and phenyl pyrenes before and after protodestannylation.

The presence of iodine atoms in diiodopyrenes Py-*n*Bu-I (**3a**) and Py-Ph-I (**3b**) quenches emission, likely due to facilitated intersystem crossing into the triplet state.[69,70] In contrast, the bis(tributylstannyl)pyrenes, Py-*n*Bu-Sn (**2a**) and Py-Ph-Sn (**2b**), are moderately fluorescent—their ~5% emission quantum yields display >50-fold increase relative to the diiodopyrenes. Interestingly, while their absorption and emission energies remain practically unperturbed by changing the R groups from *n*-butyl to phenyl, the bis-naphthyl derivative, Py-Np-Sn (**2c**), *is nearly ten times more fluorescent.* The drastic increase in the emission quantum yield is mostly derived from the enhancement in the rate of radiative decay (k_r).

The fluorescence quantum yields increase further in protodestannylated compounds **4a-b** (Py-*n*Bu-H and Py-Ph-H).The absence of Bu_3Sn groups decreases the non-radiative decay rates (k_{nr}) by nearly half relative to the Bu_3Sn-substituted counterparts **2a-b**. These observations suggest an interesting stereoelectronic scenario where the additional steric bulk by the Bu_3Sn group forces the phenyl groups out of conjugation with the central core.[71] This twisting can be clearly observed in the crystal structure of **2f'** in Scheme 6.

The fluorescence increase caused by protodestannylation is further enhanced for diphenylpyrene **4b**, where a change in conjugation accounts to a >5-fold increase in quantum yield and ~10-fold increase in *kr* relative to its n-butyl substituted counterpart, Py-nBu-H (**4a**) (Figure 1, right). Interestingly, removal of the Bu_3Sn group has a less pronounced impact on the naphthyl pair **2c**/**4c**, possibly due to the naphthyl group being too bulky to conjugate with the pyrene core even when Bu_3Sn has been removed. When compared to pyrene, the diarene substituted pyrenes **4b** and **4c** display enhanced emission with 9- and 12-fold higher quantum yields, respectively. These observations and increased k_r are symptomatic of an increased 'allowedness' of the S_1-S_0 transition. Presumably, electronic delocalization onto the non-orthogonal phenyl groups breaks the symmetry of the pyrene core and makes the photochemical transition more probable. The addition of electron donor (Py-PhOMe-H, **4d**) or acceptor (Py-PhCN-H, **4e**) groups should break the symmetry further by increasing polarization. The observation of a marked increase in the k_r and quantum yields for these molecules strengthens this hypothesis.

Benzo[*e*]pyrene **4g** resembles pyrene and benzopyrene in its photophysical behavior, albeit with a small increase in k_r. Finally, distannylperylene **2h** (Per-*t*BuPh-Sn) exhibits similar structured absorption and emission as unsubstituted perylene but with attenuated emission quantum yield and a shorter excited state lifetime. In contrast, the spectral features **4h** (Per-*t*BuPh-H) lacking the Bu_3Sn moieties, are broadened while retaining the high emission quantum yield. Overall, the presence of Bu_3Sn seems to have two substantial effects: 1) they increase steric hindrance to force orthogonality of the phenyl rings to the chromophoric core of a Per-*t*BuPh-Sn (**2h**) much more closely resembles perylene, and 2) like with the pyrene derivatives, the Bu_3Sn introduces additional vibrational relaxation pathways that increase non-radiative decay rates.

Compound	Absorbance λ (nm) [ε (×10^4 M^{-1}cm^{-1})]	Emission at rt[a]			k_r (×10^6 s^{-1})[b]	k_{nr} (×10^{7}s^{-1})[c]
		λ_{max} (nm)	τ (ns)	Φ_{PL}(%)		
Pyrene	337 [4.8]	373	–[d]	5.2	–[e]	–[e]
Py-*n*Bu-I (**3a**)	357 [5.2]	388	15.4	<0.1	–[f]	–[f]
Py-Ph-I (**3b**)	355 [4.5]	404	8.2	<0.1	–[f]	–[f]
Py-*n*Bu-Sn (**2a**)	360 [5.2]	390	11.2	5.3	4.7	8.4
Py-Ph-Sn (**2b**)	359 [3.3]	392	8.7	4.9	5.6	10.9
Py-Np-Sn (**2c**)	359 [3.9]	390	4.0	44	109.0	13.9
Py-*n*Bu-H (**4a**)	353 [4.5]	380	23.7	9.1	3.8	3.8
Py-Ph-H (**4b**)	361 [8.1]	395	10.1	47	43.5	5.6
Py-Np-H (**4c**)	353 [2.2]	403	5.3	61	115.0	7.4
Py-PhOMe-H (**4d**)	363 [4.3]	409	3.4	71	210.0	8.6
Py-PhCN-H (**4e**)	366 [1.5]	428	2.2	78	359.0	10.1
BzPy-*t*BuPh-H (**4g**)	359 [1.4]	418	9.0	26	29.1	8.3
Per-*t*BuPh-Sn (**2h**)	463 [2.1]	472	1.4	11	80.3	65.0
Per-*t*BuPh-H (**4h**)	450 [0.5]	519	7.8	89	113.0	1.4
tetra-Ph-Py **9**	359 [6.6]	411	20.6	12	5.8	4.3
Fused Py **10**	429 [3.9]	459	22.6	32	14.2	3.0

Table 2. Photophysical properties of select samples in CH_2Cl_2. [a] Emission data acquired using dilute solutions (~5×10^{-7} M). [b] $k_r = \Phi/\tau$. [c] $k_{nr} = (1-\Phi)/\tau$. [d] Pyrene's sub-nanosecond lifetime was faster than the instrument response time and was therefore unable to be measured. [e] Unable to calculate without lifetime. [f] Quantum yield was too low to give a reliable result.

Finally, when analyzing the effect of additional aryl ring substitution on the photophysics of the parent core (going from diphenylpyrene **4b** to tetra-Ph-Py **9**), the tetrasubstituted pyrene **9** has a maximum absorbance at 359 nm. The lack of a bathochromic shift hints that some of the aryl rings are out of conjugation, making this chromophore to behave as **4b**, albeit with a larger Stoke's shift (~50 nm). After Scholl cyclodehydrogenation, a ~70 nm bathochromic shift in absorbance from **9** to **10** demonstrates that the planarization allows for better electronic communication through the extended system.

Computational Analysis

Time-dependent DFT (TD-DFT) was used to evaluate the nature of excited states whereas electron density of delocalized bonds[72] (EDDB) was used to 'quantify' and visualize aromaticity in our systems. The EDDB function is derived from unperturbed one-electron densities, directly relating it to chemical resonance. The calculations were performed on a series of aryl-substituted pyrenes to investigate the effect that conjugation and the partial removal of the wavefunction symmetry constraints have on the photophysics (Scheme 10). As expected, the increase in conjugation from the aryl substituents on diphenylpyrene **4b**, when compared to pyrene (illustrated by their EDDV plots; Scheme 10), causes a ~25 nm bathochromic shift on the λ_{abs} of **4b**, as well as a marked increase in the transition probability (showcased by a ~50% increase in the magnitude of the oscillator strength). The additional conjugation for the 4-fold symmetric 1,3,6,8-tetraphenylpyrene (1,3,6,8-tetraPh-Py) follows the trend featuring a ~23 nm shift in absorbance and a 25% increase in oscillator strength from diphenylpyrene **4b**.

In contrast, for compound **9**, the conjugation from two of the aryl groups seems to be 'turned off' likely due to the presence of nodal planes on the LUMO of the pyrene's core (localized on positions 2 and 7). This is clearly observed with the EDDB plot for compound **9** where two of the phenyl groups appear orthogonal to the π-system and is further evidenced by a hypsochromic shift in its computed first excited state absorbance relative to 1,3,6,8-tetra-Ph-Py. As previously discussed, this structural feature makes the photophysics of compound **9** similar to that of a disubstituted pyrene (**4b**). Interestingly, an additional photochemical transition is allowed for **9**, likely due to its lower symmetry in comparison to 1,3,6,8-Ph-Py. Finally, after Scholl cyclization of **9**, compound **10** enjoys full conjugation throughout the polycyclic system which may be appreciated from its EDDB plot and a 59 nm red-shift in the absorbance for the first excited state (and a 31 nm shift for its third transition).

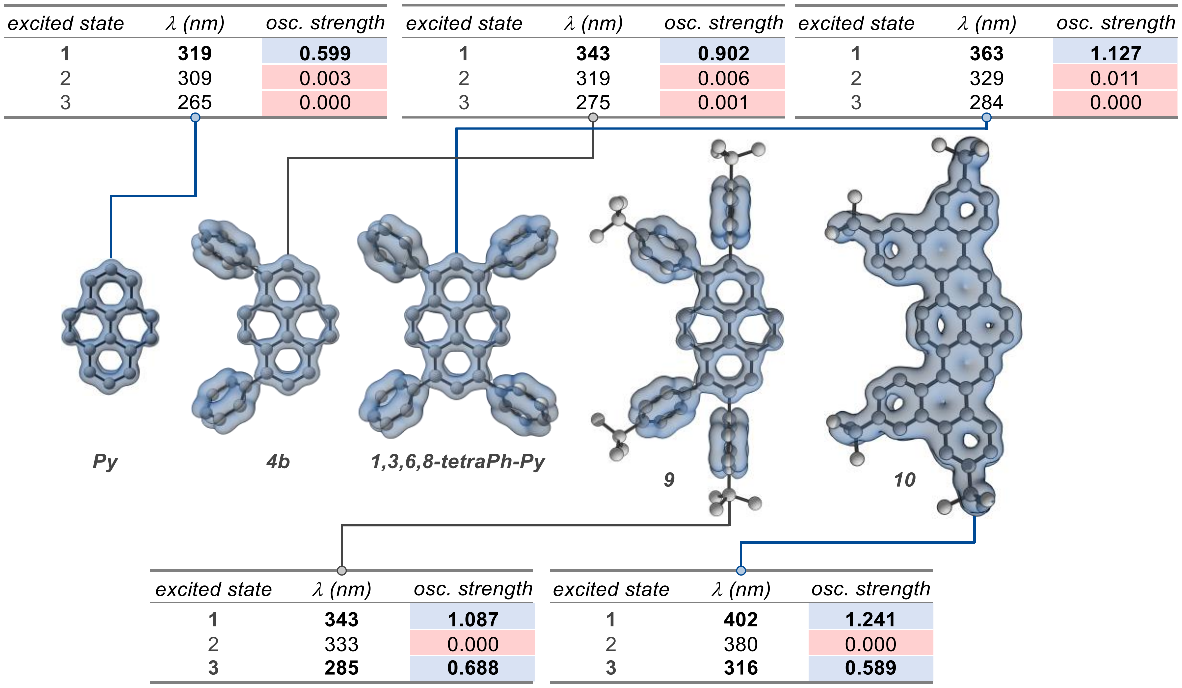

excited state	*λ (nm)*	*osc. strength*
1	**319**	**0.599**
2	309	0.003
3	265	0.000

excited state	*λ (nm)*	*osc. strength*
1	**343**	**0.902**
2	319	0.006
3	275	0.001

excited state	*λ (nm)*	*osc. strength*
1	**363**	**1.127**
2	329	0.011
3	284	0.000

excited state	*λ (nm)*	*osc. strength*
1	**343**	**1.087**
2	333	0.000
3	**285**	**0.688**

excited state	*λ (nm)*	*osc. strength*
1	**402**	**1.241**
2	380	0.000
3	**316**	**0.589**

Scheme 10. TD-DFT (tables; top and bottom) and EDDB (plots, center) computations for a series of polyarylated pyrenes performed at the TD-(SMD=DCM)/M06-2X/6-311++G(d,p) level of theory. Oscillator strengths highlighted in blue (and bold) indicate allowed transitions. Oscillator strengths highlighted in red (and not bold) indicate forbidden transitions.

Further insight into the nature of the electronic transitions involved in the observed and calculated excited state formation was obtained via analysis of MO contributions to the TD-DFT transitions. The two lowest energy transitions involve the same subsets of MOs (HOMO-1/HOMO and LUMO/LUMO+1), albeit with the different symmetry of mixing. Hence, one of these transitions is forbidden for a centrosymmetric 1,3,6,8- tetraPh-Py chromophore. The situation is drastically different for the isomeric tetra-Ph-Py **9** which lacks a center of symmetry. In the latter case, both transitions are strong (Scheme 11). These subtle but fundamentally interesting features may open new opportunities for future excited state engineering in this classic chromophore.

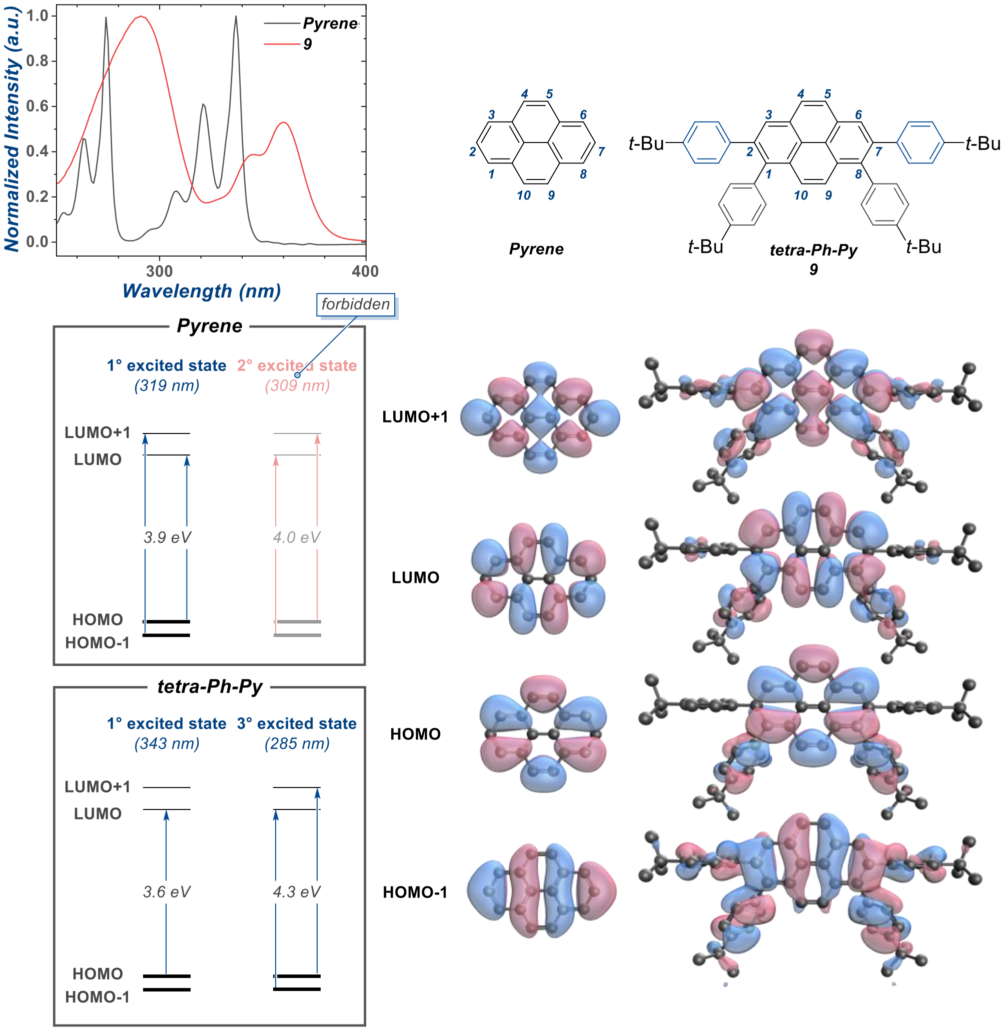

Scheme 11. Left: Molecular orbital diagrams for selected electronic transitions of Pyrene and Py-tetra-Ph-Py **9**. A forbidden transition in pyrene becomes allowed in **9** (2˚ and 3˚ excited states, respectively) as a consequence of symmetry. Right: Depiction of the HOMO-1, HOMO, LUMO, and LUMO+1 for pyrene and tetra-Ph-Py **9**.

Mechanistic Studies

Our computations compared the possible reaction mechanism for the formation of desired products and evaluated possible alternative, undesired pathways. The possible scenarios are illustrated in Scheme 12, using the naphthalene-core system as an example. All of them start with the same two steps: formation of vinyl radical **A** via R_3Sn-radical addition to one of the triple bonds followed by *peri*-cyclization on the naphthalene core to give rise to delocalized radical **B**. The difference between the top and the bottom scenarios is whether this radical can initiate another cyclization by attacking the remaining alkyne. If it can (top path), only one equivalent of the R_3SnH is needed to complete the cascade. If radical **B** is too stabilized, the radical cascade will be terminated before the second alkyne is involved. In this situation, another equivalent of R_3SnH is needed to restart the radical pathway using the 2nd alkyne moiety (i.e., the reaction follows either the central or the bottom path). If the delocalized pi-radical **B** is persistent, the final cycle formation would correspond to recombination of this radical with the new vinyl radical (central path). Alternatively, if the initially formed delocalized radicals are transformed into non-radical products, the final ring can be formed by another *peri*-annulation (bottom path).

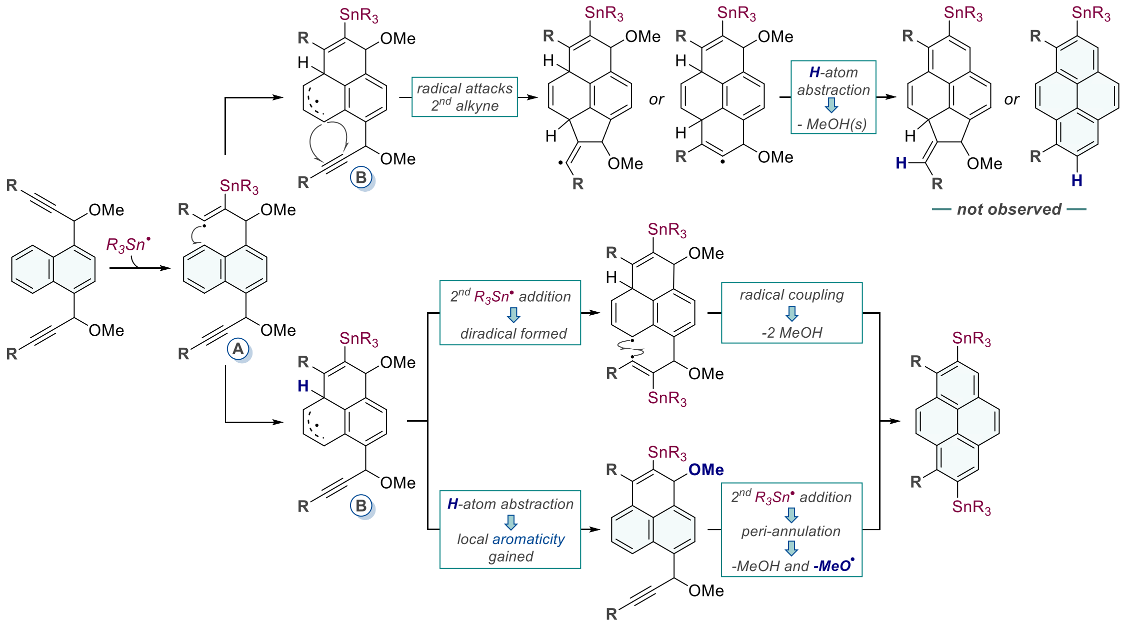

Scheme 12. Main downstream mechanistic possibilities after the Sn-radical attack on alkyne has formed the initial vinyl radical. The top cascade requires one equivalent of R_3SnH, whereas the bottom mechanisms require two equivalents of R_3SnH. Color shading denotes aromaticity.

In the following sections, we discuss several mechanistic routes that may arise from radical **B** with computed barriers and reaction energies for key steps proposed in Scheme 13. The cascade starts when vinyl radical **A** undergoes *peri*-annulation onto naphthalene giving rise to radical **B** (8.7 kcal/mol exergonic). From here, five pathways may arise as shown in Scheme 13.

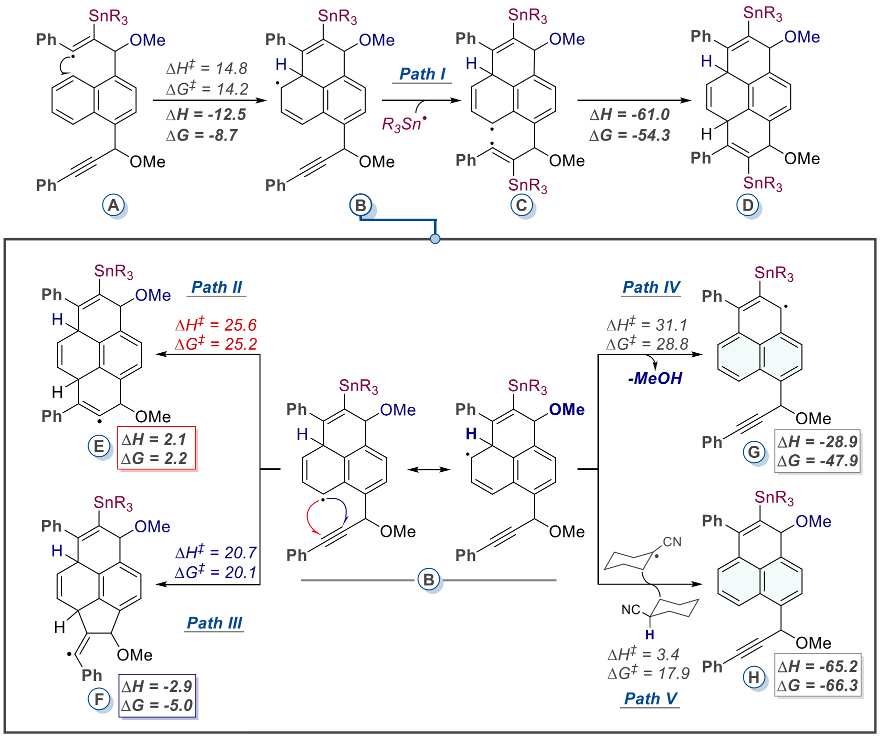

Scheme 13. Selected computations for the proposed evolution after the formation of radical **A**. Energies given in kcal/mol at the (U)M06-2X/LanL2DZ level of theory at 110 ˚C where R = Me.

Path I: Diradical annulation. Radical **B** can undergo a second Sn-radical attack at the remaining alkyne forming diradical **C**. The radical coupling of this species is calculated to be thermodynamically favorable (54.3 kcal/mol downhill) but reactions of two short-lived reactive intermediates are usually unfavorable due to their short lifetimes.[73] In the presence of an excess of ACHN-derived radicals that can convert **B** into **H**, the possibility of radical **B** being sufficiently persistent to meet the 2nd radical, arriving for this meeting from the opposite end of the molecule, is relatively low.

Paths II and III: Single-radical peri/dig annulations. As an alternative to path I, radical **B** could directly cyclize onto the second alkyne (**B** to **E** or **F**). In accordance with the stereoelectronic preferences of alkyne cyclizations,[74] formation of **F** via 5-*exo-dig* closure is calculated to be almost 10,000 times faster than the formation of **E** via a 6-*endo-dig* cyclization (~5 kcal/mol difference in the reaction barriers). From these results, only the formation of **F** seems reasonable, mainly because the formation of **E** is not only slower, but also uphill by 2.2 kcal/mol and, therefore, should be reversible. Moreover, the fact that none of the monostannyl products was observed experimentally in the reaction mixtures provides further evidence that paths II and III are not the main pathways for the reaction.

Path IV: Methanol elimination/phenalenyl radical formation. The next option is the formation of highly delocalized phenalenyl radical **G** through direct MeOH elimination from **B**. This is a highly exergonic step (48 kcal/mol downhill from **B**) due to extended conjugation of **G**. Nevertheless, it is sufficiently slow (29 kcal/mol barrier) that competing reactions may become preferred. This large kinetic barrier may be a consequence of breaking two strong bonds (C-H and C-O) in the early reactant-like transition state, before the formation of a strong OH bond is sufficiently advanced.

Path V: H-atom abstraction. The final option involves abstraction of a weak C-H bond from intermediate **B**. This process forms closed-shell intermediate **H,** which lies 66 kcal/mol below radical **B**. Furthermore, this reaction has the lowest free energy barrier (18 kcal/mol) from all the above scenarios. In addition to being the most kinetically favorable step, the involvement of the 2nd H-atom abstraction is consistent with the experimentally observed correlation between the excess of initiator and improved yields.

The combined evidence suggests path V as the preferred mechanistic pathway originating from radical **B**. The last steps displayed in Scheme 14 (from intermediate **H**) involve a second Sn-radical addition to the remaining triple bond followed by a second *peri*-annulation (intermediate **H** to **I**). In comparison to the first *peri*-annulation event (**A** to **B**), the second *peri*-annulation has a 1.2 kcal/mol lower barrier. This difference in *peri*-annulation kinetics likely derives from the phenalenyl-like intermediate being more electron-rich than naphthalene. At this point, MeO-radical elimination would form a closed-shell intermediate **J** in a nearly thermoneutral step. A second H-atom abstraction can funnel intermediate **J** into a resonance stabilized bis-allylic/benzylic radical **K** in a highly exergonic process (34 kcal/mol downhill from **J)**. Finally, radical **K** can undergo one last MeO-radical β-elimination generating the closed-shell 1,8-disubstituted-2,7-bis-stannylpyrenes.

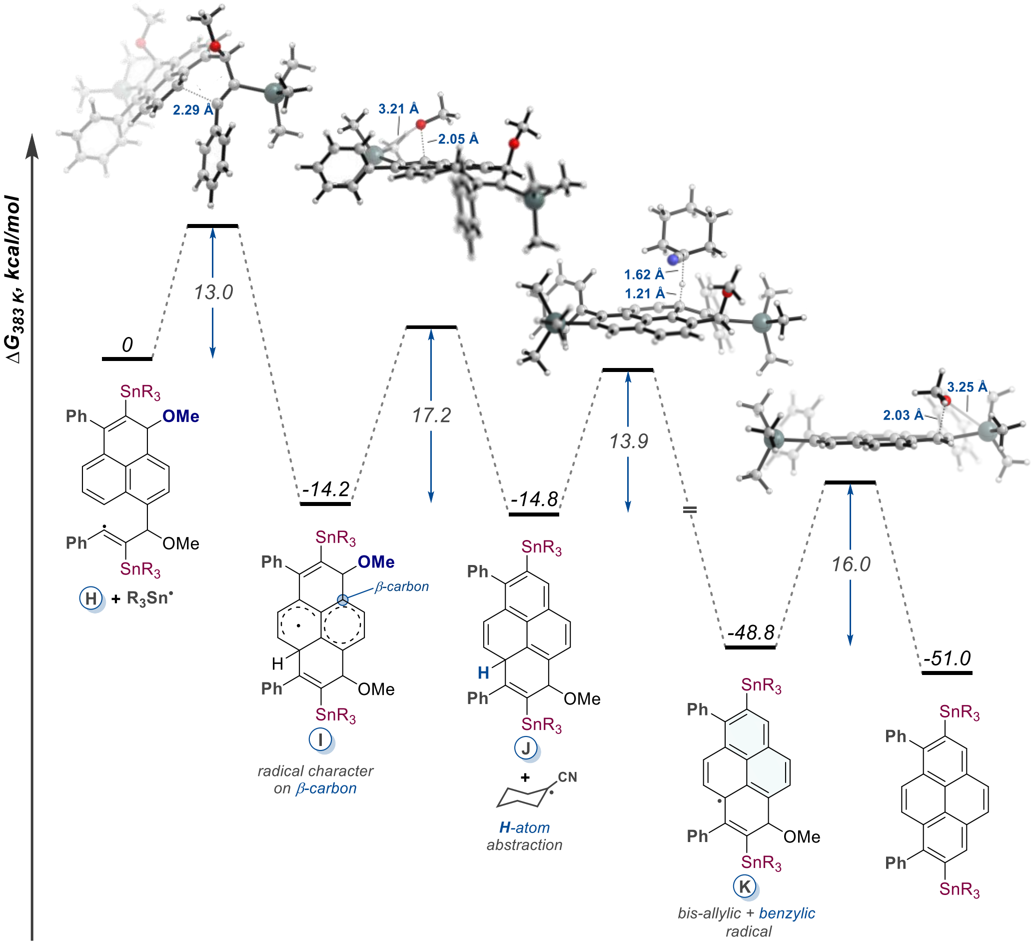

Scheme 14. Potential energy diagram and transition state geometries for the preferred reaction path from intermediate **H** to the 1,8-diphenyl-2,7-*bis*-stannylpyrene product. Energies are given in kcal/mol at the (U)M06-2X/LanL2DZ level of theory at 110˚C. $SnR_3 = SnMe_3$.

COMPUTATIONAL METHODS

DFT calculations were carried with the *Gaussian '09* software package,[75] using the (U)M06-2X DFT functional[76,77] (due to its relatively accurate description of reaction and activation energies for a variety of chemical processes including radical reactions)[78] with the LanL2DZ basis set. A broken-spin approach was used when necessary. Frequency calculations were conducted for all structures, confirming if a structure is either a minimum or a TS. Natural Bond Orbital[79–83] (NBO) analysis was performed on key structures. The Gibbs Free energy values are reported at 298 K, unless otherwise noted. Larger geometries were preoptimized with Grimme's *xtb*,[84] at the GFN2-xTB level of theory. Conformer generation and evaluation was performed with *crest*,[85] at the at the GFN2-xTB level of theory. Time-dependent DFT (at the (SMD=DCM)/UM06-2X/6-311++G(d,p) level of theory) calculations were performed on the conformers generated with *crest* to ensure a reasonable sampling of structures. Electron Density of Delocalized Bonds (EDDB)[72] calculations were performed for selected polyarenes for a description of their electronic delocalization and conjugation. These calculations were performed at the M06-2X/cc-pVTZ level of theory, with *NBO6* linked to *Gaussian '09*. Three-dimensional structures and orbital plots were produced with CYLView 1.0.1,[86] UCSF Chimera,[87] and IQMol.[88]

CONCLUSIONS

The double *peri*-annulation offers a new approach to expanding the scope of currently accessible PAHs and GNRs in a modular and straightforward manner. The structural variations that can be achieved through this approach could allow for deeper understanding and fine-tuning of PAHs' and GNRs' optoelectronic properties. The unusual substitution patterns that can be accessed by this route, in addition to the capacity for derivatization and π-extension, make this cascade useful. Furthermore, the presence of $SnBu_3$ groups offers a suite of benefits that include their solubilizing effect, direct cross-coupling potential, and the possibility for polarity reversal (through iodination). An additional benefit is the ability to use a change in media acidity as a precipitation and fluorescence intensity enhancement tool through protodestannylation.

This approach can be extended to triple *peri*-annulations where *peri*-annulations are coupled with a radical cascade that connects two preexisting aromatic cores via a formal C-H activation step. For example, two naphthyl moieties can be fused into a perylene core en route to the final peropyrene product. In this cascade, ACHN-derived radicals play a dual role as both radical initiators and oxidants.

Photophysical studies revealed interesting trends suggesting multiple effects of the bulky Bu_3Sn groups. Their presence restricts rotation of adjacent aryl moieties, forcing them out of conjugation and introduces additional vibrational relaxation pathways that increase non-radiative decay rates. Removal of Sn groups by treatment with acid 'turns on' fluorescence while their substitution with iodine quenches it. In comparison to pyrene, some of our diarylpyrenes display >10-fold enhancement in their fluorescence quantum yield. Furthermore, TD-DFT and EDDB calculations revealed the impact of the non-centrosymmetric substitution pattern on the electronic structure and the nature of excited states.

DFT computations were used to unravel the complicated mechanistic nature of the double *peri*-annulation reaction. Computations also helped explain why monostannyl side products were not observed as products for this transformation.

ASSOCIATED CONTENT

S Supporting Information.

Full experimental details, ^1H NMR, ^{13}C NMR spectra for all the prepared compounds, X-ray crystallographic data for selected products, and computational details for all calculated structures. This material is available free of charge via the Internet at http://pubs.acs.org.

AUTHOR INFORMATION

§ Current affiliation: Department of Chemistry and Department of Computer Science, University of Toronto, ON, Canada.
§§ Current affiliation: Los Alamos National Laboratory, Los Alamos, NM, United States.

Corresponding Author

* alabugin@chem.fsu.edu

ACKNOWLEDGMENTS

E.G.-R. is thankful for the support provided by CONACYT throughout his graduate studies. Financial support of this work by the National Science Foundation is gratefully acknowledged (CHE-1800329). Computational resources were provided by NSF XSEDE (TG-CHE160006) and FSU Research Computing Center. G.P.G. thanks Professor Alán Aspuru-Guzik (University of Toronto) for the support.

REFERENCES

(1) Chen, L.; Hernandez, Y.; Feng, X.; Müllen, K. From Nanographene and Graphene Nanoribbons to Graphene Sheets: Chemical Synthesis. *Angew. Chem., Int. Ed.* **2012**, *51* (31), 7640–7654. https://doi.org/10.1002/anie.201201084.

(2) Son, Y.-W.; Cohen, M. L.; Louie, S. G. Half-Metallic Graphene Nanoribbons. *Nature* **2006**, *444* (7117), 347–349. https://doi.org/10.1038/nature05180.

(3) Schwierz, F. Graphene Transistors. *Nat. Nanotechnol.* **2010**, *5* (7), 487–496. https://doi.org/10.1038/nnano.2010.89.

(4) Geim, A. K.; Novoselov, K. S. The Rise of Graphene. *Nat. Mater.* **2007**, *6* (3), 183–191. https://doi.org/10.1038/nmat1849.

(5) Wu, J.; Pisula, W.; Müllen, K. Graphenes as Potential Material for Electronics. *Chem. Rev.* **2007**, *107* (3), 718–747. https://doi.org/10.1021/cr068010r.

(6) Allen, M. J.; Tung, V. C.; Kaner, R. B. Honeycomb Carbon: A Review of Graphene. *Chem. Rev.* **2010**, *110* (1), 132–145. https://doi.org/10.1021/cr900070d.

(7) Kim, S.; Kim, B.; Lee, J.; Shin, H.; Park, Y.-I.; Park, J. Design of Fluorescent Blue Light-Emitting Materials Based on Analyses of Chemical Structures and Their Effects. *Mater. Sci. Eng., R* **2016**, *99*, 1–22. https://doi.org/10.1016/J.MSER.2015.11.001.

(8) Wöhrle, T.; Wurzbach, I.; Kirres, J.; Kostidou, A.; Kapernaum, N.; Litterscheidt, J.; Haenle, J. C.; Staffeld, P.; Baro, A.; Giesselmann, F.; Laschat, S. Discotic Liquid Crystals. *Chem. Rev.* **2016**, *116* (3), 1139–1241. https://doi.org/10.1021/acs.chemrev.5b00190.

(9) Mei, J.; Diao, Y.; Appleton, A. L.; Fang, L.; Bao, Z. Integrated Materials Design of Organic Semiconductors for Field-Effect Transistors. *J. Am. Chem. Soc.* **2013**, *135* (18), 6724–6746. https://doi.org/10.1021/ja400881n.

(10) Pisula, W.; Feng, X.; Müllen, K. Tuning the Columnar Organization of Discotic Polycyclic Aromatic Hydrocarbons. *Adv. Mater.* **2010**, *22* (33), 3634–3649. https://doi.org/10.1002/adma.201000585.

(11) Ritter, K. A.; Lyding, J. W. The Influence of Edge Structure on the Electronic Properties of Graphene Quantum Dots and Nanoribbons. *Nat. Mater.* **2009**, *8* (3), 235–242. https://doi.org/10.1038/nmat2378.

(12) Rieger, R.; Müllen, K. Forever Young: Polycyclic Aromatic Hydrocarbons as Model Cases for Structural and Optical Studies. *J. Phys. Org. Chem.* **2010**, *23* (4), n/a-n/a. https://doi.org/10.1002/poc.1644.

(13) Kim, S.; Hwang, S. W.; Kim, M.-K.; Shin, D. Y.; Shin, D. H.; Kim, C. O.; Yang, S. B.; Park, J. H.; Hwang, E.; Choi, S.-H.; Ko, G.; Sim, S.; Sone, C.; Choi, H. J.; Bae, S.; Hong, B. H.

Anomalous Behaviors of Visible Luminescence from Graphene Quantum Dots: Interplay between Size and Shape. *ACS Nano* **2012**, *6* (9), 8203–8208. https://doi.org/10.1021/nn302878r.

(14) Sun, Z.; Ye, Q.; Chi, C.; Wu, J. Low Band Gap Polycyclic Hydrocarbons: From Closed-Shell near Infrared Dyes and Semiconductors to Open-Shell Radicals. *Chem. Soc. Rev.* **2012**, *41* (23), 7857. https://doi.org/10.1039/c2cs35211g.

(15) Liu, J.; Li, B.-W.; Tan, Y.-Z.; Giannakopoulos, A.; Sanchez-Sanchez, C.; Beljonne, D.; Ruffieux, P.; Fasel, R.; Feng, X.; Müllen, K. Toward Cove-Edged Low Band Gap Graphene Nanoribbons. *J. Am. Chem. Soc.* **2015**, *137* (18), 6097–6103. https://doi.org/10.1021/jacs.5b03017.

(16) Itami, K. Toward Controlled Synthesis of Carbon Nanotubes and Graphenes. *Pure Appl. Chem.* **2012**, *84* (4), 907–916. https://doi.org/10.1351/PAC-CON-11-11-15.

(17) von Kugelgen, S.; Piskun, I.; Griffin, J. H.; Eckdahl, C. T.; Jarenwattananon, N. N.; Fischer, F. R. Templated Synthesis of End-Functionalized Graphene Nanoribbons through Living Ring-Opening Alkyne Metathesis Polymerization. *J. Am. Chem. Soc.* **2019**, *141* (28), 11050–11058. https://doi.org/10.1021/jacs.9b01805.

(18) Steiner, A.-K.; Amsharov, K. Y. The Rolling-Up of Oligophenylenes to Nanographenes by a HF-Zipping Approach. *Angew. Chem., Int. Ed.* **2017**, *56* (46), 14732–14736. https://doi.org/10.1002/anie.201707272.

(19) Kolmer, M.; Zuzak, R.; Steiner, A. K.; Zajac, L.; Engelund, M.; Godlewski, S.; Szymonski, M.; Amsharov, K. Fluorine-Programmed Nanozipping to Tailored Nanographenes on Rutile TiO_2 Surfaces. *Science* **2019**, *363* (6422), 57–60. https://doi.org/10.1126/SCIENCE.AAV4954.

(20) Rogers, C.; Chen, C.; Pedramrazi, Z.; Omrani, A. A.; Tsai, H.-Z.; Jung, H. S.; Lin, S.; Crommie, M. F.; Fischer, F. R. Closing the Nanographene Gap: Surface-Assisted Synthesis of Peripentacene from 6,6′-Bipentacene Precursors. *Angew. Chem., Int. Ed.* **2015**, *54* (50), 15143–15146. https://doi.org/10.1002/anie.201507104.

(21) Bronner, C.; Marangoni, T.; Rizzo, D. J.; Durr, R. A.; Jørgensen, J. H.; Fischer, F. R.; Crommie, M. F. Iodine versus Bromine Functionalization for Bottom-Up Graphene Nanoribbon Growth: Role of Diffusion. *J. Phys. Chem. C* **2017**, *121* (34), 18490–18495. https://doi.org/10.1021/acs.jpcc.7b02896.

(22) Nguyen, G. D.; Tsai, H.-Z.; Omrani, A. A.; Marangoni, T.; Wu, M.; Rizzo, D. J.; Rodgers, G. F.; Cloke, R. R.; Durr, R. A.; Sakai, Y.; Liou, F.; Aikawa, A. S.; Chelikowsky, J. R.; Louie, S. G.; Fischer, F. R.; Crommie, M. F. Atomically Precise Graphene Nanoribbon Heterojunctions from a Single Molecular Precursor. *Nat. Nanotechnol.* **2017**, *12* (11), 1077–1082. https://doi.org/10.1038/nnano.2017.155.

(23) Rizzo, D. J.; Veber, G.; Cao, T.; Bronner, C.; Chen, T.; Zhao, F.; Rodriguez, H.; Louie, S. G.; Crommie, M. F.; Fischer, F. R. Topological Band Engineering of Graphene Nanoribbons. *Nature* **2018**, *560* (7717), 204–208. https://doi.org/10.1038/s41586-018-0376-8.

(24) Segawa, Y.; Ito, H.; Itami, K. Structurally Uniform and Atomically Precise Carbon Nanostructures. *Nat. Rev. Mater.* **2016**, *1* (1), 15002. https://doi.org/10.1038/natrevmats.2015.2.

(25) Yang, X.; Dou, X.; Rouhanipour, A.; Zhi, L.; Räder, H. J.; Müllen, K. Two-Dimensional Graphene Nanoribbons. *J. Am. Chem. Soc.* **2008**, *130* (13), 4216–4217. https://doi.org/10.1021/ja710234t.

(26) Narita, A.; Feng, X.; Hernandez, Y.; Jensen, S. A.; Bonn, M.; Yang, H.; Verzhbitskiy, I. A.; Casiraghi, C.; Hansen, M. R.; Koch, A. H. R.; Fytas, G.; Ivasenko, O.; Li, B.; Mali, K. S.; Balandina, T.; Mahesh, S.; De Feyter, S.; Müllen, K. Synthesis of Structurally Well-Defined and Liquid-Phase-Processable Graphene Nanoribbons. *Nat. Chem.* **2014**, *6* (2), 126–132. https://doi.org/10.1038/nchem.1819.

(27) Ito, H.; Ozaki, K.; Itami, K. Annulative π-Extension (APEX): Rapid Access to Fused Arenes, Heteroarenes, and Nanographenes. *Angew. Chem., Int. Ed.* **2017**, *56* (37), 11144–11164. https://doi.org/10.1002/anie.201701058.

(28) Matsuoka, W.; Ito, H.; Itami, K. Rapid Access to Nanographenes and Fused Heteroaromatics by Palladium-Catalyzed Annulative π-Extension Reaction of Unfunctionalized Aromatics with Diiodobiaryls. *Angew. Chem., Int. Ed.* **2017**, *56* (40), 12224–12228. https://doi.org/10.1002/anie.201707486.

(29) Ozaki, K.; Murai, K.; Matsuoka, W.; Kawasumi, K.; Ito, H.; Itami, K. One-Step Annulative π-Extension of Alkynes with Dibenzosiloles or Dibenzogermoles by Palladium/o-Chloranil Catalysis. *Angew. Chem., Int. Ed.* **2017**, *56* (5), 1361–1364. https://doi.org/10.1002/anie.201610374.

(30) Ito, H.; Segawa, Y.; Murakami, K.; Itami, K. Polycyclic Arene Synthesis by Annulative π-Extension. *J. Am. Chem. Soc.* **2019**, *141* (1), 3–10. https://doi.org/10.1021/jacs.8b09232.

(31) Yano, Y.; Mitoma, N.; Matsushima, K.; Wang, F.; Matsui, K.; Takakura, A.; Miyauchi, Y.; Ito, H.; Itami, K. Living Annulative π-Extension Polymerization for Graphene Nanoribbon Synthesis. *Nature* **2019**, *571* (7765), 387–392. https://doi.org/10.1038/s41586-019-1331-z.

(32) Asao, N.; Tsutomu, N.; Lee, S.; Yamamoto, Y. Lewis Acid-Catalyzed Benzannulation via Unprecedented [4+2] Cycloaddition of o-Alkynyl(oxo)Benzenes and Enynals with Alkynes. **2003**. https://doi.org/10.1021/JA036927R.

(33) Reetz, M. T.; Sommer, K. Gold-Catalyzed Hydroarylation of Alkynes. *Eur. J. Org. Chem.* **2003**, *2003* (18), 3485–3496. https://doi.org/10.1002/ejoc.200300260.

(34) Yang, W.; Bam, R.; Catalano, V. J.; Chalifoux, W. A. Highly Regioselective Domino Benzannulation Reaction of Buta-1,3-Diynes to Construct Irregular Nanographenes. *Angew. Chem., Int. Ed.* **2018**, *57* (45), 14773–14777. https://doi.org/10.1002/anie.201808043.

(35) Senese, A. D.; Chalifoux, W. A. Nanographene and Graphene Nanoribbon Synthesis via Alkyne Benzannulations. *Molecules* **2019**, *24* (1), 118. https://doi.org/10.3390/molecules24010118.

(36) Alabugin, I. V.; Gonzalez-Rodriguez, E. Alkyne Origami: Folding Oligoalkynes into Polyaromatics. *Acc. Chem. Res.* **2018**, *51* (5), 1206–1219. https://doi.org/10.1021/acs.accounts.8b00026.

(37) Alabugin, I.; Gonzalez-Rodriguez, E.; Kawade, R.; Stepanov, A.; Vasilevsky, S. Alkynes as Synthetic Equivalents of Ketones and Aldehydes: A Hidden Entry into Carbonyl Chemistry. *Molecules* **2019**, *24* (6), 1036. https://doi.org/10.3390/molecules24061036.

(38) Nevado, C.; Echavarren, A. M. Transition Metal-Catalyzed Hydroarylation of Alkynes. *Synthesis* **2005**, *2*, 167–182. https://doi.org/10.1055/s-2005-861781.

(39) Nevado, C.; Echavarren, A. M. Intramolecular Hydroarylation of Alkynes Catalyzed by Platinum or Gold: Mechanism and endo Selectivity. *Chem. - Eur. J.* **2005**, *11* (10), 3155–3164. https://doi.org/10.1002/chem.200401069.

(40) Li, C. W.; Wang, C. I.; Liao, H. Y.; Chaudhuri, R.; Liu, R. S. Synthesis of Dibenzo[*g,p*]Chrysenes from Bis(biaryl)Acetylenes via Sequential ICl-Induced Cyclization and Mizoroki-Heck Coupling. *J. Org. Chem.* **2007**, *72* (24), 9203–9207. https://doi.org/10.1021/jo701504m.

(41) Arslan, H.; Saathoff, J. D.; Bunck, D. N.; Clancy, P.; Dichtel, W. R. Highly Efficient Benzannulation of Poly(phenylene ethynylene)s. *Angew. Chem., Int. Ed.* **2012**, *51* (48), 12051–12054. https://doi.org/10.1002/anie.201206964.

(42) Dou, C.; Saito, S.; Gao, L.; Matsumoto, N.; Karasawa, T.; Zhang, H.; Fukazawa, A.; Yamaguchi, S. Sequential Electrophilic and Photochemical Cyclizations from Bis(bithienyl)Acetylene to a Tetrathienonaphthalene Core. *Org. Lett.* **2013**, *15* (1), 80–83. https://doi.org/10.1021/ol303107y.

(43) Arslan, H.; Uribe-Romo, F. J.; Smith, B. J.; Dichtel, W. R. Accessing Extended and Partially Fused Hexabenzocoronenes Using a Benzannulation–Cyclodehydrogenation Approach. *Chem. Sci.* **2013**, *4* (10), 3973. https://doi.org/10.1039/c3sc51212f.

(44) Yang, W.; Lucotti, A.; Tommasini, M.; Chalifoux, W. A. Bottom-Up Synthesis of Soluble and Narrow Graphene Nanoribbons Using Alkyne Benzannulations. *J. Am. Chem. Soc.* **2016**, *138* (29), 9137–9144. https://doi.org/10.1021/jacs.6b03014.

(45) Yang, W.; Chalifoux, W. Rapid π-Extension of Aromatics via Alkyne Benzannulations. *Synlett* **2017**, *28* (06), 625–632. https://doi.org/10.1055/s-0036-1588688.

(46) Nun, P.; Gaillard, S.; Poater, A.; Cavallo, L.; Nolan, S. P. A Combined Mechanistic and Computational Study of the Gold(I)-Catalyzed Formation of Substituted Indenes. *Org. Biomol. Chem.* **2011**, *9* (1), 101–104. https://doi.org/10.1039/C0OB00758G.

(47) For *peri*-annulations with other functional groups: Holt, C. J.; Wentworth, K. J.; Johnson, R. P. A Short and Efficient Synthesis of the [3]Triangulene Ring System. *Angew. Chem., Int. Ed.* **2019**, *58* (44), 15793–15796. https://doi.org/10.1002/anie.201907226.

(48) Tsvetkov, N. P.; Gonzalez-Rodriguez, E.; Hughes, A.; dos Passos Gomes, G.; White, F. D.; Kuriakose, F.; Alabugin, I. V. Radical Alkyne *Peri*-Annulation Reactions for the Synthesis of Functionalized Phenalenes, Benzanthrenes, and Olympicene. *Angew. Chem., Int. Ed.* **2018**, *57* (14), 3651–3655. https://doi.org/10.1002/anie.201712783.

(49) Pati, K.; dos Passos Gomes, G.; Harris, T.; Hughes, A.; Phan, H.; Banerjee, T.; Hanson, K.; Alabugin, I. V. Traceless Directing Groups in Radical Cascades: From Oligoalkynes to Fused Helicenes without Tethered Initiators. *J. Am. Chem. Soc.* **2015**, *137* (3), 1165–1180. https://doi.org/10.1021/ja510563d.

(50) Pati, K.; dos Passos Gomes, G.; Alabugin, I. V. Combining Traceless Directing Groups with Hybridization Control of Radical Reactivity: From Skipped Enynes to Defect-Free Hexagonal Frameworks. *Angew. Chem., Int. Ed.* **2016**, *55* (38), 11633–11637. https://doi.org/10.1002/anie.201605799.

(51) Hughes, A. M.; dos Passos Gomes, G.; Alabugin, I. V. Stereoelectronic Influence of a “Spectator” Propargylic Substituent can Override Aromaticity Effects in Radical *Peri*-Cyclizations en Route to Expanded Polyaromatics. *J. Org. Chem.* **2019**, *84* (4), 1853–1862. https://doi.org/10.1021/acs.joc.8b02779.

(52) Zhou, Z.; Kawade, R. K.; Wei, Z.; Kuriakose, F.; Üngör, Ö.; Jo, M.; Shatruk, M.; Gershoni-Poranne, R.; Petrukhina, M. A.; Alabugin, I. V. Negative Charge as a Lens for Concentrating Antiaromaticity: Using a Pentagonal “Defect” and Helicene Strain for Cyclizations. *Angew. Chem., Int. Ed.* **2020**, *59* (3), 1256–1262. https://doi.org/10.1002/anie.201911319.

(53) Pati, K.; Michas, C.; Allenger, D.; Piskun, I.; Coutros, P. S.; Gomes, G. dos P.; Alabugin, I. V. Synthesis of Functionalized Phenanthrenes via Regioselective Oxidative Radical Cyclization. *J. Org. Chem.* **2015**, *80* (23), 11706–11717. https://doi.org/10.1021/acs.joc.5b01014.

(54) Hale, K. J.; Manaviazar, S.; Watson, H. A. The O-Directed Free Radical Hydrostannation of Propargyloxy Dialkyl Acetylenes with Ph_3SnH/Cat. Et_3B. A Refutal of the Stannylvinyl Cation Mechanism. *Chem. Rec.* **2019**, *19* (2–3), 238–319. https://doi.org/10.1002/tcr.201700104.

(55) Dimopoulos, P.; George, J.; Tocher, D. A.; Manaviazar, S.; Hale, K. J. Mechanistic Studies on the O-Directed Free-Radical Hydrostannation of Disubstituted Acetylenes with Ph_3SnH and Et_3B and on the Iodination of Allylically Oxygenated α-Triphenylstannylalkenes. *Org. Lett.* **2005**, *7* (24), 5377–5380. https://doi.org/10.1021/ol051937d.

(56) Hale, K. J.; Grabski, M.; Manaviazar, S.; Maczka, M. Asymmetric Total Synthesis of (+)-Inthomycin C via O-Directed Free Radical Alkyne Hydrostannation with Ph_3SnH and Catalytic Et_3B: Reinstatement of the Zeeck–Taylor (3R)-Structure for (+)-Inthomycin C. *Org. Lett.* **2014**, *16* (4), 1164–1167. https://doi.org/10.1021/ol5000499.

(57) Watson, H. A.; Manaviazar, S.; Steeds, H. G.; Hale, K. J. Fast Ring-Opening of an Intermediary α-Stannyl-β-Cyclopropylvinyl Radical does not Support Formation of an α-Stannylvinyl Cation in the O-Directed Free Radical Hydrostannation of Dialkyl Acetylenes. *Chem. Commun.* **2019**, *55* (96), 14454–14457. https://doi.org/10.1039/c9cc05492h.

(58) Hale, K. J.; Maczka, M.; Kaur, A.; Manaviazar, S.; Ostovar, M.; Grabski, M. Synthesis of the C(7)–C(22) Sector of (+)-Acutiphycin via O-Directed Double Free Radical Alkyne Hydrostannation with Ph_3SnH/Et_3B, Double I–Sn Exchange, and Double Stille Coupling. *Org. Lett.* **2014**, *16* (4), 1168–1171. https://doi.org/10.1021/ol500050p.

(59) Manaviazar, S.; Hale, K. J.; LeFranc, A. Enantioselective Formal Total Synthesis of the Dendrobatidae Frog Toxin, (+)-Pumiliotoxin B, via O-Directed Alkyne Free Radical Hydrostannation. *Tetrahedron Lett.* **2011**, *52* (17), 2080–2084. https://doi.org/10.1016/J.TETLET.2010.10.141.

(60) Dimopoulos, P.; Athlan, A.; Manaviazar, S.; George, J.; Walters, M.; Lazarides, L.; Aliev, A. E.; Hale, K. J. O-Directed Free-Radical Hydrostannations of Propargyl Ethers, Acetals, and Alcohols with Ph_3SnH and Et_3B. *Org. Lett.* **2005**, *7* (24), 5369–5372. https://doi.org/10.1021/ol051936l.

(61) Grimshaw, J.; Trocha-Grimshaw, J. Characterisation of 1,6- and 1,8-Dibromopyrenes. *J. Chem. Soc. Perkin Trans. 1* **1972**, 1622. https://doi.org/10.1039/p19720001622.

(62) Koga, Y.; Kaneda, T.; Saito, Y.; Murakami, K.; Itami, K. Synthesis of Partially and Fully Fused Polyaromatics by Annulative Chlorophenylene Dimerization. *Science* **2018**, *359* (6374), 435–439. https://doi.org/10.1126/science.aap9801.

(63) Yang, W.; Monteiro, J. H. S. K.; de Bettencourt-Dias, A.; Catalano, V. J.; Chalifoux, W. A. Pyrenes, Peropyrenes, and Teropyrenes: Synthesis, Structures, and Photophysical Properties. *Angew. Chem., Int. Ed.* **2016**, *55* (35), 10427–10430. https://doi.org/10.1002/anie.201604741.

(64) Yang, W.; Monteiro, J. H. S. K.; de Bettencourt-Dias, A.; Chalifoux, W. A. New Thiophene-Functionalized Pyrene, Peropyrene, and Teropyrene via a Two- or Four-Fold Alkyne Annulation and their Photophysical Properties. *Can. J. Chem.* **2017**, *95* (4), 341–345. https://doi.org/10.1139/cjc-2016-0466.

(65) Figueira-Duarte, T. M.; Müllen, K. Pyrene-Based Materials for Organic Electronics. *Chem. Rev.* **2011**, *111* (11), 7260–7314. https://doi.org/10.1021/cr100428a.

(66) Aparin, I. O.; Proskurin, G. V.; Golovin, A. V.; Ustinov, A. V.; Formanovsky, A. A.; Zatsepin, T. S.; Korshun, V. A. Fine Tuning of Pyrene Excimer Fluorescence in Molecular Beacons by Alteration of the Monomer Structure. *J. Org. Chem.* **2017**, *82* (19), 10015–10024. https://doi.org/10.1021/acs.joc.7b01451.

(67) Nichols, V. M.; Rodriguez, M. T.; Piland, G. B.; Tham, F.; Nesterov, V. N.; Youngblood, W. J.; Bardeen, C. J. Assessing the Potential of Peropyrene as a Singlet Fission Material: Photophysical Properties in Solution and the Solid State. *J. Phys. Chem. C* **2013**, *117* (33), 16802–16810. https://doi.org/10.1021/jp4051116.

(68) Nagami, T.; Ito, S.; Kubo, T.; Nakano, M. Intermolecular Packing Effects on Singlet Fission in Oligorylene Dimers. *ACS Omega* **2017**, *2* (8), 5095–5103. https://doi.org/10.1021/acsomega.7b00655.

(69) Martinho, J. M. G. Heavy-Atom Quenching of Monomer and Excimer Pyrene Fluorescence. *J. Phys. Chem.* **1989**, *93* (18), 6687–6692. https://doi.org/10.1021/j100355a024.

(70) However, attempts at observing phosphorescent emission at 77K were unsuccessful.

(71) For another example where the steric bulk of the Bu_3Sn group has chemical consequences, see: Harris, T.; Gomes, G. D. P.; Clark, R. J.; Alabugin, I. V. Domino Fragmentations in Traceless Directing Groups of Radical Cascades: Evidence for the Formation of Alkoxy Radicals via C-O Scission. *J. Org. Chem.* **2016**, *81* (14), 6007–6017. https://doi.org/10.1021/acs.joc.6b01052.

(72) Szczepanik, D. W.; Andrzejak, M.; Dominikowska, J.; Pawełek, B.; Krygowski, T. M.; Szatylowicz, H.; Solà, M. The Electron Density of Delocalized Bonds (EDDB) Applied for Quantifying Aromaticity. *Phys. Chem. Chem. Phys.* **2017**, *19* (42), 28970–28981. https://doi.org/10.1039/c7cp06114e.

(73) At this level of theory, the calculated activation energy for C→D as a triplet is $\Delta\mathrm{G}^{\neq} = 27.1$ kcal/mol ($\Delta\mathrm{H}^{\neq} = 24.3$ kcal/mol). It is important to note that accurate calculations of singlet diradical species by DFT methods can be challenging. Although the reaction through a singlet pathway (possibly with significant zwitterionic character) that would be inherently faster, his path also suffers from including two short-lived reactive intermediates.

(74) Gilmore, K.; Mohamed, R. K.; Alabugin, I. V. The Baldwin Rules: Revised and Extended. *Wiley Interdiscip. Rev. Comput. Mol. Sci.* **2016**, *6* (5), 487–514. https://doi.org/10.1002/wcms.1261.

(75) M. J. Frisch, G.; Trucks, W.; Schlegel, H. B. .; Scuseria, G. E. .; Robb, M. A. .; Cheeseman, J. R.; Scalmani, G.; Barone, V. .; Mennucci, B. .; Petersson, G. A.; Nakatsuji, H.; Caricato, M. .; Li, X. .; Hratchian, H. P. .; Izmaylov, A. F. .; Bloino, J. .; Zheng, G. .; Sonnenberg, J. L. .; Frisch, M. J.; Trucks, G. W. .; Schlegel, H. B. .; Scuseria, G. E. .; Robb, M. A. .; Cheeseman, J. R.; Scalmani, G. .; Barone, V. .; Mennucci, B. .; Petersson, G. A.; Nakatsuji, H. .; Caricato, M. .; Li, X. .; Hratchian, H. P. .; Izmaylov, A. F. .; Bloino, J. .; Zheng, G. .; Sonnenberg, J. L. .; Hada, M.; Ehara, M.; Toyota, K. .; Fukuda, R. .; Hasegawa, J. .; Ishida, M. .; Nakajima, T. .; Honda, Y. .; Kitao, O. .; Nakai, H. .; Vreven, T. .; Montgomery, J. A., Jr.; Peralta, J. E. .; Ogliaro, F. .; Bearpark, M. .; Heyd, J. J. .; Brothers, E. .; Kudin, K. N. .; Staroverov, V. N.; Kobayashi, R. .; Normand, J.; Raghavachari, K. .; Rendell, A. .; Burant, J. C. .; Iyengar, S. S. .; Tomasi, J. .; Cossi, M. .; Rega, N. .; Millam, J. M. .; Klene, M. .; Knox, J. E. .; Cross, J. B. .; Bakken, V. .; Adamo, C. .; Jaramillo, J. .; Gomperts, R. .; Stratmann, R. E. .; Yazyev, O. .; Austin, A. J. .; Cammi, R. .; Pomelli, C. .; Ochterski, J. W. .; Martin, R. L. .; Morokuma, K. .; Zakrzewski, V. G. .; Voth, G. A. .; Salvador, P. .; Dannenberg, J. J.; Dapprich, S. .; Daniels, A. D. .; Farkas, Ö. .; Foresman, J. B. .; Ortiz, J. V. .; Cioslowski, J. .; Fox, D. J. *Gaussian 09, Gaussian, Inc., Wallingford CT*; 2009.

(76) Zhao, Y.; Truhlar, D. G. The M06 Suite of Density Functionals for Main Group Thermochemistry, Thermochemical Kinetics, Noncovalent Interactions, Excited States, and Transition Elements: Two New Functionals and Systematic Testing of Four M06-Class Functionals and 12 Other Functionals. *Theor. Chem. Acc.* **2008**, *120* (1–3), 215–241. https://doi.org/10.1007/s00214-007-0310-x.

(77) Zhao, Y.; Truhlar, D. G. Density Functionals with Broad Applicability in Chemistry. *Acc. Chem. Res.* **2008**, *41* (2), 157–167. https://doi.org/10.1021/ar700111a.

(78) Zhao, Y.; Truhlar, D. G. How Well Can New-Generation Density Functionals Describe the Energetics of Bond-Dissociation Reactions Producing Radicals? *J. Phys. Chem. A* **2008**, *112* (6), 1095–1099. https://doi.org/10.1021/jp7109127.

(79) Weinhold, F.; Landis, C. R.; Glendening, E. D. What Is NBO Analysis and How Is It Useful? *International Reviews in Physical Chemistry*. Taylor and Francis Ltd. July 2, 2016, pp 399–440. https://doi.org/10.1080/0144235X.2016.1192262.

(80) Reed, A. E.; Weinhold, F. Natural Localized Molecular Orbitals. *J. Chem. Phys.* **1985**, *83* (4), 1736–1740. https://doi.org/10.1063/1.449360.

(81) Reed, A. E.; Weinhold, F. Natural Bond Orbital Analysis of Internal Rotation Barriers and Related Phenomena. *Isr. J. Chem.* **1991**, *31* (4), 277–285. https://doi.org/10.1002/ijch.199100032.

(82) Reed, A. E.; Curtiss, L. A.; Weinhold, F. Intermolecular Interactions from a Natural Bond Orbital, Donor-Acceptor Viewpoint. *Chem. Rev.* **1988**, *88* (6), 899–926. https://doi.org/10.1021/cr00088a005.

(83) Weinhold, F. Natural Bond Orbital Methods in: P.v.R. Schleyer. In *Encyclopedia of Computational Chemistry*; 1998; pp 1793–1810.

(84) Grimme, S.; Bannwarth, C.; Shushkov, P. A Robust and Accurate Tight-Binding Quantum Chemical Method for Structures, Vibrational Frequencies, and Noncovalent Interactions of Large Molecular Systems Parametrized for All Spd-Block Elements (Z = 1-86). *J. Chem. Theory Comput.* **2017**, *13* (5), 1989–2009. https://doi.org/10.1021/acs.jctc.7b00118.

(85) Grimme, S. Exploration of Chemical Compound, Conformer, and Reaction Space with Meta-Dynamics Simulations Based on Tight-Binding Quantum Chemical Calculations. *J. Chem. Theory Comput.* **2019**, *15* (5), 2847–2862. https://doi.org/10.1021/acs.jctc.9b00143.

(86) Legault, C. Y. CYLview, 1.0b. *Univ. Sherbrooke* **2009**.

(87) Pettersen, E. F.; Goddard, T. D.; Huang, C. C.; Couch, G. S.; Greenblatt, D. M.; Meng, E. C.; Ferrin, T. E. UCSF Chimera-A Visualization System for Exploratory Research and Analysis. *J. Comput. Chem.* **2004**, *25* (13), 1605–1612. https://doi.org/10.1002/jcc.20084.

(88) IQMol 2.13; http://www.iqmol.org (Accessed January 2020).

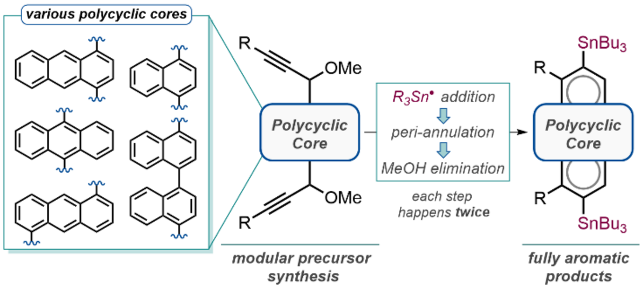

(.PNG)

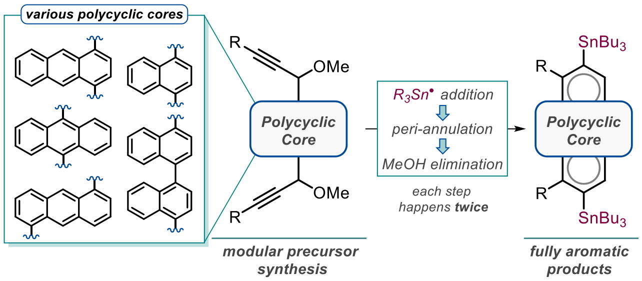

(ChemDraw)